Nanocomposites of few-layer graphene oxide and alumina by density functional theory calculations

Jonathan M. Polfus[a*], Ole Martin Løvvik[a], Per Martin Rørvik[a], Rune Bredesen[a]

[a]SINTEF Materials and Chemistry, Forskningsveien 1, NO-0314 Oslo, Norway

Keywords: graphene oxide; Al2O3; nanocomposite; interface; DFT

Abstract

The atomistic and electronic structure and oxygen stoichiometry of nanocomposites between alumina and graphene oxide were investigated by density functional theory calculations. The nanocomposite was described as interfaces between α-Al_2O_3 (0001) surfaces and graphene oxide; the latter was defined with oxygen bound as epoxy groups and a C:O atomic ratio of 4:1. The optimized composite structure with 1-3 layers of graphene oxide in between Al_2O_3 contains bridging Al-O-C bonds at the interface. Reduction of the composite was investigated by removal of oxygen from the interface Al-O-C bonds, within the graphene oxide layers and in Al_2O_3. It was found that removal of oxygen within the graphene oxide layers is essentially independent of the Al_2O_3 interface, i.e., the same as in pure graphene oxide. Oxygen was, however, more strongly bound in the interface Al-O-C bonds by 0.80 eV, and reduction of graphene oxide to graphene is accordingly preferred within the graphene oxide layers rather than at the oxide interface.

1. Introduction

Composites between graphitic materials and metal oxides have the potential to exhibit complementary functional properties of the constituents: graphitic materials exhibit exceptional electrical, thermal, optical and mechanical properties, whereas metal oxides can act as a mechanically and chemically robust matrix with synergistic dielectric or semiconducting properties [1,2]. Such composites can for instance be used as conductive material for high-temperature applications and thermoelectric devices [3], photocatalyst for water splitting [4] and electrode material in lithium ion batteries [5] and electrochemical capacitors [6].

*Corresponding author. E-mail: jonathan.polfus@sintef.no (Jonathan M. Polfus)

Graphene oxide (GO) has emerged as an important graphitic material in particular as it can be produced from graphite by cost-effective chemical methods and is easily dispersed in water; GO can therefore be processed via a range of techniques of commercial viability [7,8]. Thermal or chemical reduction of GO is necessary to regain the desirable properties of pristine graphene, at least to some extent. While GO with saturated sp^3 carbon is an insulator, reduced GO can reach electrical conductivities similar to graphite, i.e., two orders of magnitude lower than graphene. GO is nonetheless an interesting material in itself, e.g., as a catalyst [9], water membrane [10], or for sensing applications [7]. Furthermore, for interfaces between graphene and metal oxides, bonds may form between oxide ions in the metal oxide and graphene, and GO structures should accordingly be considered in determining the properties of such interfaces [11].

Fan et al. [12] recently prepared nanocomposites between Al_2O_3 and graphene with GO as precursor and simultaneous reduction and densification via spark plasma sintering. The nanocomposite contained α-Al_2O_3 grains encompassed by a few graphene layers which were well dispersed in the ceramic matrix, and exhibited an electrical conductivity of 10^3 S m^{-1} for an estimated 2.35 vol.% graphene. Furthermore, it was reported that the charge carrier type changed from p-type to n-type as the graphene content increased. The mechanical and microstructural properties of such nanocomposites have also been reported [13,14].

The interface between α-Al_2O_3 (0001) and pristine graphene has been investigated computationally to elucidate its atomistic and electronic structure [11,15,16]. Several other interfaces between graphene and metal oxides or semiconductors have been studied by computational approaches including ZnO, MgO, SiO_2 and SiC [17–21]. On the other hand, computational studies involving GO tend to focus on structural aspects of the isolated material due to the significant non-stoichiometry and disorder present – (reduced) graphene oxide can refer to a plenitude of compositions and structures depending on its synthesis procedure and treatment [22]. It is therefore important to study interfaces with GO due to its increased use as graphitic material.

The major functional groups in GO are epoxy, hydroxyl and carbonyl on the basal plane of the graphene sheet, and carboxyl at the edges [22]. The functional groups are randomly distributed and their concentration is highly variable. Upon thermal reduction of GO, significant mass loss occurs as CO, CO_2 and H_2O is released, e.g., 60 and 85 % under Ar flow at 300 and 1300 °C, respectively [12]. Bagri et al. [23] found epoxy groups to be prevalent among the remaining oxygen groups for most initial configurations after annealing at 1000-1500 K by molecular dynamics simulations.

In the present work, we have investigated interfaces between GO and Al_2O_3 (0001) surfaces in order to understand the structural properties and chemical bonds in the nanocomposites. Structural models were constructed and optimized with respect to the distribution of oxygen groups in GO and lateral position of GO relative to Al_2O_3 (0001). Furthermore, the electronic structure and energetics of oxygen removal was considered in the Al_2O_3 and GO parts of the composite material to determine whether reduction of the nanocomposites behave differently from that of GO. The C:O ratio was fixed to 4:1 in the reference state, which represents prepared GO or weakly reduced GO depending on the preparation method [7,8]. Further oxygen removal therefore corresponds to a mild or initial reduction, and is not associated with mass loss as CO_2.

2. Computational procedures

DFT calculations were performed using the projector-augmented wave (PAW) method [24,25] as implemented in VASP [26–28]. The generalized gradient approximation due to Perdew, Burke and Ernzerhof [29] (GGA-PBE) was employed for obtaining a suitable structural model of the Al_2O_3–GO interface. Final calculations of atomistic and electronic structure and energetics were performed with the hybrid functional due to Heyd, Scuseria, and Ernzerhof [30] with a screening factor of 0.2 (HSE). Hybrid functionals – intermixing 25% exact Hartree-Fock exchange – provide significantly improved band gaps, band edge positions and defect levels for semiconductors and insulators including metal oxides [31,32]. The van der Waals forces that are of significant importance for graphene structures were taken into account through the semi empirical correction scheme due to Grimme [33] (DFT+D2). This approach has been successfully applied for describing geometries of graphene-related structures [34,35], and interfaces between graphene and metal oxides [11,16,18–20].

Calculations were performed with a 500 eV plane-wave energy cut-off and a 4×4×1 k-point sampling for the rhombohedral α-Al_2O_3 unit cell. Atomic positions and cell parameters were optimized until the residual forces for the relaxed atoms were within 0.02 eV $Å^{-1}$ with a self-consistency energy convergence of 10^{-6} eV. The Al_2O_3 (0001) surface was constructed as an Al-terminated slab of 12 Al-layers and 6 O_3-layers, i.e., the same size as the $R\bar{3}c$ unit cell, and with a 25 Å vacuum layer between the periodic images of the slab. Structural and electronic properties have been shown to be converged for the same 18-layer surface slab [36].

GO models were constructed from 2×2 graphene cells with a C:O ratio of 4:1 and oxygen bound as epoxy groups on each side of the graphene sheets in various configurations. Epoxy is among the prevalent oxygen groups (in addition to hydroxyl and edge groups) characterized experimentally and reported to be among the most stable in computational studies [9,23,37–39].

Composite cells were constructed with 1 and 3 identical parallel layers of GO in between Al_2O_3 (0001) surfaces. The *a* and *b* cell parameters were fixed to those of the relaxed Al_2O_3 cell – an approach corresponding to the GO material adapting to a fixed Al_2O_3 matrix by compressive strain in the GO layers. Interfaces with (tensile) strained graphene have been shown to offer an essentially equivalent description of electronic properties that do not depend significantly on the exact geometry of the graphene layer [40]. The lateral positions of the GO layers were optimized by translation along the *a* and *b* lattice vectors. For the model with 3 GO layers, the GO layers adjoining the Al_2O_3 (0001) surfaces were kept geometrically equivalent while the lateral position of the middle GO layer was optimized separately.

Reduction of the composite was investigated by considering the energetics of oxygen removal from various sites in 2×2×1 supercells (240 atoms). As such, the stability of *oxygen vacancies* was considered in the composite model with a C:O ratio of 4:1 in the GO layers as the reference state. Oxygen vacancies associated with the GO part of the composite cell are accompanied by a change in hybridization from sp^3 to sp^2 in GO and are therefore not effectively charged as in typical ceramic materials. In the Al_2O_3 part of the composite, oxygen takes an oxidation state of -2 and a vacancy therefore yielded two excess electrons in the GO states close to the valence band maximum (VBM) of Al_2O_3. Due to the considerable difference in the chemical environment of oxygen in the Al_2O_3 and GO parts of the composite, initial GGA-PBE calculation were performed to evaluate the most stable sites and final calculations were performed with HSE and a convergence criteria of 0.05 eV $Å^{-1}$.

The charge of oxide ions in the Al_2O_3, GO and interface part of the composite cell was evaluated by Bader analysis of the charge density [41]. The enthalpy of oxidation of graphene to GO, i.e., energy of dissociative chemisorption of O_2 on graphene, was calculated according to

$$\Delta E^{\mathrm{ox}} = E^{\mathrm{tot}}_{\mathrm{GO}} - E^{\mathrm{tot}}_{\mathrm{Graphene}} - nE^{\mathrm{tot}}_{\mathrm{O_2}} \quad (1)$$

where E_{GO}^{tot} and $E_{Graphene}^{tot}$ are the total energies of the GO and the graphene cells, respectively, $E_{O_2}^{tot}$ is the total energy of the spin-polarized O_2 molecule, and n is half the number of oxygen in GO.

3. Results and discussion

3.1 Structure of bulk, surface and composite models

The calculated lattice parameters of bulk α-Al_2O_3, a = 4.755 Å, c = 12.985 Å, were within 0.2 % of experimental values at room temperature [42], and the relaxed structure of the α-Al_2O_3 (0001) surface was in excellent agreement with other computational studies; the outer Al ion relaxed inward by 0.74 Å forming an approximate trigonal planar AlO_3 coordination (Figure 1) and the surface energy is 1.52 J m^{-2} [36,43,44]. The calculated band gap of α-Al_2O_3 was 8.15 eV (direct) which compares well with the experimental (optical) band gap, 8.8 eV [45]. For the (0001) surface, the band gap is reduced to 6.37 eV and a similar lowering of the band gap is reported by GGA-PBE calculations [44].

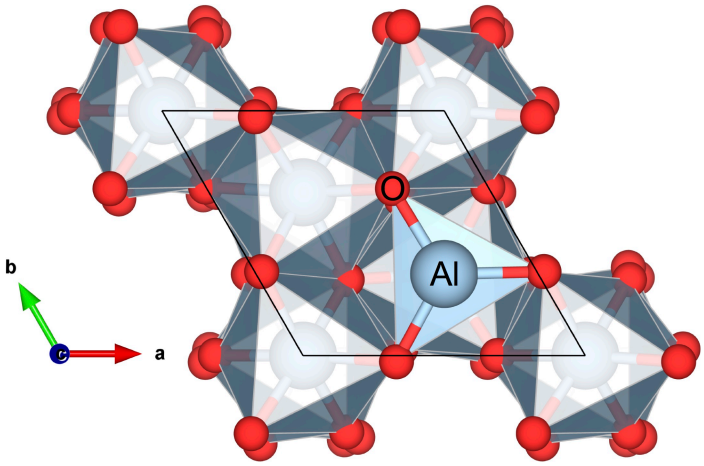

Figure 1: Relaxed structure of the α-Al_2O_3 0001 unit cell showing a trigonal planar AlO_3 unit at the surface.

Figure 2 shows the relaxed structure of three GO models with different configurations of oxygen as epoxy groups on both sides of the graphene sheet and a C:O ratio of 4:1. The configuration in Figure 2a was more stable than those in b and c by 0.34 and 0.27 eV per C_8O_2 cell, respectively. The lattice parameter of the most stable relaxed GO cell (Figure 2a) was 5.05 Å, compared to 4.90 Å for a 2×2 graphene cell, in accordance with expansion of the C-C bond length from 1.42 Å in graphene to 1.47 Å in the epoxy groups of GO, in line with similar DFT calculations [39,46]. The carbon atoms of the epoxy groups are relaxed out from

the graphene plane and thereby introduce a roughness in the carbon structure of GO of up to 0.36 Å.

The compressive strain induced in the GO layer when adapted to the Al_2O_3 cell amounts to 6.3 %. Upon optimizing the lateral position of the GO layer with respect to the Al_2O_3 surface, lowest energy was obtained when the oxygen in the GO layer formed a bridging bond directly to the outer aluminium ion of the Al_2O_3 surface (see Figure 4). This corresponds to translation of the GO layer by $\frac{1}{8}$ and $\frac{1}{12}$ along the *a* and *b* vectors of the Al_2O_3 unit cell, respectively.

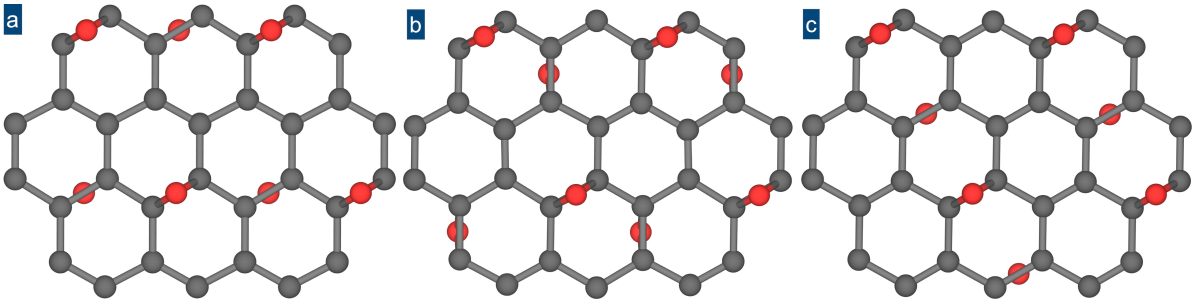

Figure 2: Relaxed structure of three different GO cells with a C:O ratio of 4:1 and oxygen bound as epoxy groups on both sides of the graphene sheet. The configuration in (a) was more stable than those in (b) and (c) by 0.34 and 0.27 eV, respectively, for C_8O_2 cells.

A relaxed composite model with 1 GO layer is shown in Figure 3. Due to the symmetrical constraints of the computational cell, bridging Al-O-C bonds on both sides of GO was only possible with the less stable GO configuration in Figure 2c. The surface aluminium ion has relaxed outward closer to its bulk position and the epoxy and Al-O bond lengths of the bridging unit are essentially unchanged relative to isolated GO and bulk Al_2O_3. While the roughness in the carbon structure of the GO layers increased slightly to 0.56 Å, it is still rather low compared to, e.g., 1.47 Å reported for an interface between graphene and MgO (111) [18].

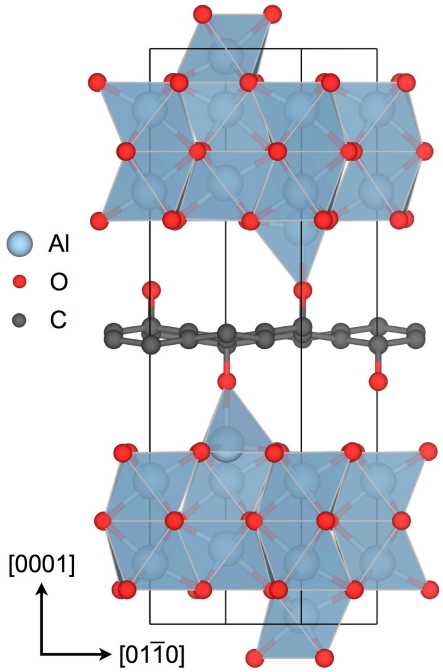

Figure 3: Relaxed structure of a composite model with 1 GO layer. The epoxy groups in the GO layer are arranged as in Figure 2c (C:O ratio of 4:1).

For the composite model with 3 GO layers (Al_2O_3-3GO), shown in Figure 4, the interface GO layers are equivalent with respect to the Al_2O_3 surfaces, and the most stable GO configuration was used (Figure 2a). It was found that the middle GO layer was rather insensitive to lateral position in terms of energy as long the epoxy groups of adjacent layers did not come too close to each other. The most stable configuration was obtained by translating the middle GO layer $\frac{1}{8}$ along the *a* vector of the Al_2O_3 cell while several other configurations were only 6-18 meV higher in energy per C_8O_2 layer. The interlayer GO distance is reported to vary with oxygen content, i.e., from 3.35 Å for graphite to around 8 Å for graphite oxide [47]. With an intermediate amount of oxygen and high degree of order, the calculated interlayer GO distance, 4.1 Å, compares well with experimental values for reduced GO, e.g., 3.57-4.3 Å [47–49]. The roughness in the carbon structure of the GO layers, 0.43 Å, is slightly lower than for the 1 GO layer model (see Figure 3). It may be noted that relaxation energy of the compressively strained GO, i.e., the energy difference between the strained and unstrained GO cell, amounts to 0.48 eV per C_8O_2 layer.

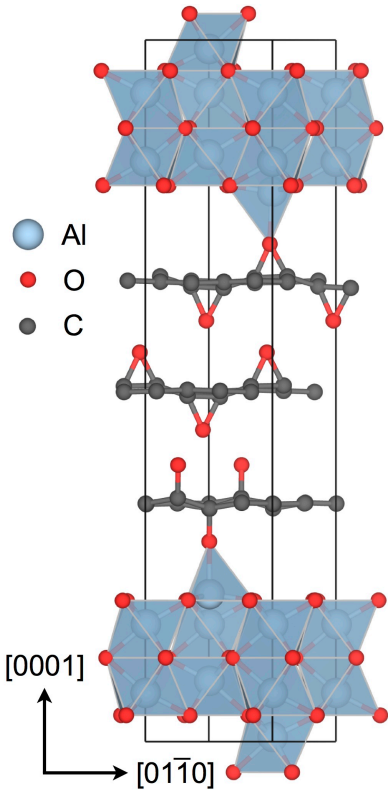

Figure 4: Relaxed structure of the composite model with 3 GO layers in between α-Al_2O_3 0001 surfaces (Al_2O_3-3GO). The GO layers have identical epoxy group configuration (C:O ratio of 4:1), and the interface GO layers are equivalent with respect to the Al_2O_3 surface.

3.2 Electronic structure

The electronic density of states (DOS) for the Al_2O_3 (0001) surface, 3-layer GO (3GO) and the 3-layer composite (Al_2O_3-3GO) is shown in Figure 5. Changes in the Al_2O_3 and GO related states of the composite are quite subtle compared to the isolated materials. The occupancy of the states close to VBM is however quite different; the composite cell exhibits partial occupancy below VBM and otherwise unoccupied states in isolated 3GO are partially occupied in the composite. A minor charge transfer from Al_2O_3 to 3GO was confirmed by Bader charge analysis: the average charge of the bridging Al-O-C oxygen was -1.30 in the composite while it was -1.12 and -1.13 in the GO part of the composite and in the isolated 3GO cell, respectively. (The average charge of oxygen in Al_2O_3 in both the isolated and composite cells was -1.99, corresponding to a fully ionized charge state). Accordingly, it seems that the minor charge transfer from Al_2O_3 to GO is limited to the chemical bond of the bridging Al-O-C unit and therefore does not influence the concentrations of electron or hole carriers in the nanocomposite. The n-type and p-type doping effects observed by Fan et al. [12] can therefore not be explained by the electronic structure of the pristine interface considered in the present work.

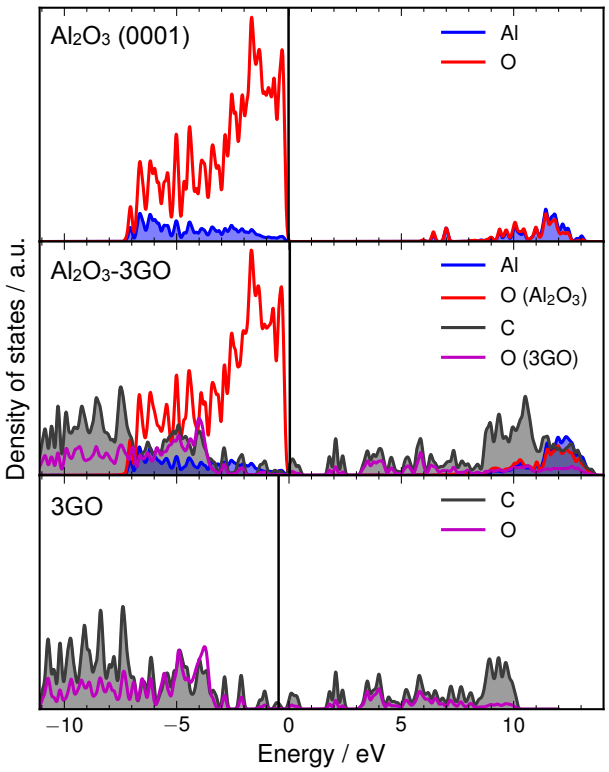

Figure 5: Site projected electronic density of states of Al_2O_3 (0001) surface (top), 3GO (bottom) and the composite (middle). The energy scale is referenced to the VBM of Al_2O_3, and C core-states in 3GO were aligned to 3GO in the composite. The vertical lines indicate the highest partly occupied states. It can be seen that the VBM of Al_2O_3 (0001) is higher in energy than the highest occupied states in 3GO.

The relation between oxygen associated with Al_2O_3, GO and the bridging Al-O-C bonds is illustrated in Figure 6. The oxygen states related to the bridging Al-O-C bonds exhibit a rather similar electronic character as the other 3GO oxygen states. The occupied oxygen states associated with Al-O-C are, however, shifted to lower energy compared to the 3GO states (e.g., lower intensity at -4 eV in Figure 6), indicating that the bridging oxygen are more strongly bound and more stable.

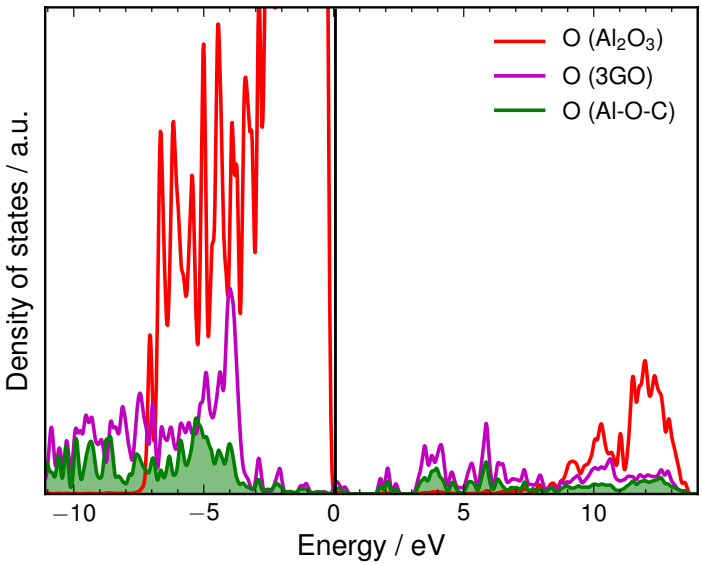

Figure 6: Site projected electronic density of states of oxygen associated with Al_2O_3, 3GO and the Al-O-C bridging bond in the composite model. The highest partly occupied states are slightly above the VBM of Al_2O_3, which is referenced to 0 eV.

3.3 Reduction and oxygen stoichiometry

Initial GGA calculations showed that while oxygen vacancies in the Al_2O_3 part of the composite cell were more stable in the surface layer than in bulk by 1.15 eV, vacancies in the GO part of the composite were more stable by up to 2.63 eV. Furthermore, the stability of oxygen vacancies on the two non-equivalent sites in the GO part of the 3-layer composite (excluding Al-O-C) were essentially the same (within 0.01 eV). HSE calculations were therefore focused towards the two most stable oxygen vacancies in the 3-layer composite, i.e., for the bridging Al-O-C oxygen and within the GO layers of the composite. The vacancy stability was also considered for the isolated 3GO cell for comparison.

Figure 7 shows the relaxed structure of 240 atom cells with an oxygen vacancy in the Al-O-C bond (a) and within the GO layers of the composite (b), corresponding to an increase in the C:O ratio to 4.57:1. Removal of oxygen breaks the symmetry of the cell and introduces significant distortion in the GO layers in comparison to the reference model in Figure 4. The roughness in the carbon structure increases up to 1.3 Å. Removal of oxygen was found to be more favorable in the GO layer than in the Al-O-C bond by 0.80 eV. In comparison, the enthalpy of oxidation of graphene to GO was calculated to 0.44 eV for a C_8O_2 unit (Figure 2c) relative to pristine graphene, or 0.22 eV per O. Accordingly, the difference in stability of oxygen vacancies between the GO layer and the bridging Al-O-C unit is significant, and reduction can be expected to principally occur within the GO layers. Considering the significant distortion in the vacancy cells, it should be noted that the difference in vacancy

stability can have contributions from relaxation due to strain and the symmetrical constraints of the cell.

The calculated oxygen vacancy stability on equivalent sites in Al_2O_3-3GO and an isolated 3GO model was found to be essentially the same. Thus, reduction of GO in Al_2O_3 nanocomposites can be expected to be thermodynamically similar to isolated GO except for the bridging Al-O-C bonds. This indicates that removal of oxygen from the GO layers in Al_2O_3-GO composites by reduction, to increase for instance the electrical conductivity, can be done without sacrificing bonding between the Al_2O_3 surface and the closest GO layer; thus maintaining the microstructural morphology of the composite.

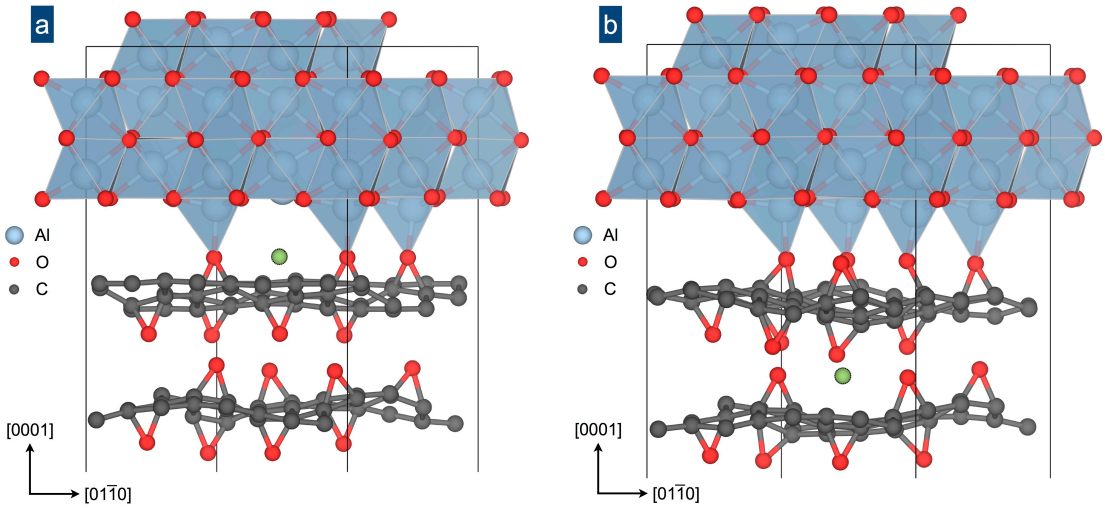

Figure 7: Relaxed structure with oxygen removed from the Al-O-C bond (a), and from within the GO layers in Al_2O_3-3GO (b). The original position of the removed oxygen is shown with a green sphere and the lower part of the computational cell is not shown.

4. Conclusions

Nanocomposite structures of α-Al_2O_3 and graphene oxide with a C:O atomic ratio of 4:1 and with oxygen bound as epoxy groups were constructed and optimized. The optimized structure with 1 and 3 graphene oxide layers contains strong Al-O-C bonds bridging the interface to the (0001) surface of Al_2O_3. The electronic structure of the composite showed partially occupied states associated with GO at the Fermi level. Reduction of the material was investigated in terms of the energetics of oxygen removal from the graphene oxide, Al_2O_3 and the Al-O-C interface bond of the composite. Oxygen removal was found to be significantly more favorable within the graphene oxide layers by 0.80 and 1.48 eV compared to the Al-O-C and Al_2O_3 part of the composite, respectively. Reduction can therefore be expected to principally occur within the graphene oxide layers of the nanocomposite, while keeping the bridging

oxygen and bond between the two phases. The properties of the interface Al-O-C bonds can be expected to be essentially independent of the number of GO layers in the nanocomposite.

5. Acknowledgement

The authors are grateful for computational resources provided through the Norwegian Metacenter for Computational Science (NOTUR) under the project nn9259k.

6. References

[1] Wu Z-S, Zhou G, Yin L-C, Ren W, Li F, Cheng H-M. Graphene/metal oxide composite electrode materials for energy storage. Nano Energy 2012;1:107–31.

[2] Porwal H, Grasso S, Reece MJ. Review of graphene–ceramic matrix composites. Adv Appl Ceram 2013;112:443–54.

[3] Jankovský O, Šimek P, Sedmidubský D, Huber Š, Pumera M, Sofer Z. Towards highly electrically conductive and thermally insulating graphene nanocomposites: Al_2O_3 – graphene. RSC Adv 2014;4:7418–24.

[4] Meng FK, Li JT, Cushing SK, Bright J, Zhi MJ, Rowley JD, et al. Photocatalytic Water Oxidation by Hematite/Reduced Graphene Oxide Composites. Acs Catal 2013;3:746–51.

[5] Wang H, Cui L-F, Yang Y, Sanchez Casalongue H, Robinson JT, Liang Y, et al. Mn_3O_4-graphene hybrid as a high-capacity anode material for lithium ion batteries. J Am Chem Soc 2010;132:13978–80.

[6] Yan J, Fan Z, Wei T, Qian W, Zhang M, Wei F. Fast and reversible surface redox reaction of graphene–MnO_2 composites as supercapacitor electrodes. Carbon 2010;48:3825–33.

[7] Perrozzi F, Prezioso S, Ottaviano L. Graphene oxide: from fundamentals to applications. J Phys Condens Matter 2015;27:013002.

[8] Pei S, Cheng H-M. The reduction of graphene oxide. Carbon 2012;50:3210–28.

[9] Boukhvalov DW, Dreyer DR, Bielawski CW, Son Y-W. A Computational Investigation of the Catalytic Properties of Graphene Oxide: Exploring Mechanisms by using DFT Methods. ChemCatChem 2012;4:1844–9.

[10] Nair RR, Wu HA, Jayaram PN, Grigorieva I V, Geim AK. Unimpeded permeation of water through helium-leak-tight graphene-based membranes. Science (80-) 2012;335:442–4.

[11] Huang B, Xu Q, Wei S-H. Theoretical study of corundum as an ideal gate dielectric material for graphene transistors. Phys Rev B 2011;84:155406.

[12] Fan Y, Jiang W, Kawasaki A. Highly Conductive Few-Layer Graphene/Al_2O_3 Nanocomposites with Tunable Charge Carrier Type. Adv Funct Mater 2012;22:3882–9.

[13] Fan Y, Estili M, Igarashi G, Jiang W, Kawasaki A. The effect of homogeneously dispersed few-layer graphene on microstructure and mechanical properties of Al_2O_3 nanocomposites. J Eur Ceram Soc 2014;34:443–51.

[14] Centeno A, Rocha VG, Alonso B, Fernández A, Gutierrez-Gonzalez CF, Torrecillas R, et al. Graphene for tough and electroconductive alumina ceramics. J Eur Ceram Soc 2013;33:3201–10.

[15] Ilyasov V V., Ershov I V. Surface states and adsorption energy of carbon in the interface of the two-dimensional graphene/Al_2O_3(0001) system. Phys Solid State 2012;54:2335–43.

[16] Cho S, Lee S, Chung Y. Water Trapping at the Graphene/Al_2O_3 Interface. Jpn J Appl Phys 2013;52:06GD09.

[17] Xu P, Tang Q, Zhou Z. Structural and electronic properties of graphene-ZnO interfaces: dispersion-corrected density functional theory investigations. Nanotechnology 2013;24:305401.

[18] Cho SB, Chung Y-C. Bandgap engineering of graphene by corrugation on lattice-mismatched MgO (111). J Mater Chem C 2013;1:1595.

[19] Cho SB, Chung Y-C. Spin-polarized bandgap of graphene induced by alternative chemisorption with MgO (111) substrate. Carbon 2014;77:208–14.

[20] Fan XF, Zheng WT, Chihaia V, Shen ZX, Kuo J-L. Interaction between graphene and the surface of SiO2. J Phys Condens Matter 2012;24:305004.

[21] Varchon F, Feng R, Hass J, Li X, Nguyen B. Electronic structure of epitaxial graphene layers on SiC: effect of the substrate. Phys Rev Lett 2007;99:126805.

[22] Mao S, Pu H, Chen J. Graphene oxide and its reduction: modeling and experimental progress. RSC Adv 2012;2:2643.

[23] Bagri A, Mattevi C, Acik M, Chabal YJ, Chhowalla M, Shenoy VB. Structural evolution during the reduction of chemically derived graphene oxide. Nat Chem 2010;2:581–7.

[24] Blöchl PE. Projector augmented-wave method. Phys Rev B 1994;50:17953–79.

[25] Kresse G, Joubert D. From ultrasoft pseudopotentials to the projector augmented-wave method. Phys Rev B 1999;59:1758–75.

[26] Kresse G, Hafner J. Ab initio molecular dynamics for liquid metals. Phys Rev B 1993;47:558–61.

[27] Kresse G, Hafner J. Ab initio molecular-dynamics simulation of the liquid-metal-amorphous-semiconductor transition in germanium. Phys Rev B 1994;49:14251–69.

[28] Kresse G. Efficiency of ab-initio total energy calculations for metals and semiconductors using a plane-wave basis set. Comput Mater Sci 1996;6:15–50.

[29] Perdew J, Burke K, Ernzerhof M. Generalized Gradient Approximation Made Simple. Phys Rev Lett 1996;77:3865–8.

[30] Heyd J, Scuseria GE, Ernzerhof M. Erratum: “Hybrid functionals based on a screened Coulomb potential” [J. Chem. Phys. 118, 8207 (2003)]. J Chem Phys 2006;124:219906.

[31] Paier J, Marsman M, Hummer K, Kresse G, Gerber IC, Angyán JG. Screened hybrid density functionals applied to solids. J Chem Phys 2006;124:154709.

[32] Alkauskas A, Broqvist P, Pasquarello A. Defect levels through hybrid density functionals: Insights and applications. Phys Status Solidi 2011;248:775–89.

[33] Grimme S. Semiempirical GGA-type density functional constructed with a long-range dispersion correction. J Comput Chem 2006;16:1787–99.

[34] Mercurio G, McNellis ER, Martin I, Hagen S, Leyssner F, Soubatch S, et al. Structure and Energetics of Azobenzene on Ag(111): Benchmarking Semiempirical Dispersion Correction Approaches. Phys Rev Lett 2010;104:036102.

[35] Stradi D, Barja S, Díaz C, Garnica M, Borca B, Hinarejos JJ, et al. Role of Dispersion Forces in the Structure of Graphene Monolayers on Ru Surfaces. Phys Rev Lett 2011;106:186102.

[36] Baltrusaitis J, Hatch C, Orlando R. Electronic Properties and Reactivity of Simulated Fe^{3+} and Cr^{3+} Substituted α-Al_2O_3 (0001) Surface. J Phys Chem C 2012;116:18847−18856.

[37] Lerf A, He H, Forster M, Klinowski J. Structure of Graphite Oxide Revisited ‖. J Phys Chem B 1998;102:4477–82.

[38] Pandey D, Reifenberger R, Piner R. Scanning probe microscopy study of exfoliated oxidized graphene sheets. Surf Sci 2008;602:1607–13.

[39] Andre Mkhoyan K, Contryman AW, Silcox J, Stewart D a, Eda G, Mattevi C, et al. Atomic and electronic structure of graphene-oxide. Nano Lett 2009;9:1058–63.

[40] Stradi D, Barja S, Díaz C, Garnica M, Borca B, Hinarejos J, et al. Lattice-matched versus lattice-mismatched models to describe epitaxial monolayer graphene on Ru(0001). Phys Rev B 2013;88:245401.

[41] Tang W, Sanville E, Henkelman G. A grid-based Bader analysis algorithm without lattice bias. J Phys Condens Matter 2009;21:084204.

[42] Thompson P, Cox DE, Hastings JB. Rietveld refinement of Debye–Scherrer synchrotron X-ray data from Al_2O_3. J Appl Crystallogr 1987;20:79–83.

[43] Rohmann C, Metson JB, Idriss H. Surface Science DFT study of carbon monoxide adsorption on α -Al_2O_3 (0001). Surf Sci 2011;605:1694–703.

[44] Rohmann C, Metson J, Idriss H. DFT study of carbon monoxide adsorption on hydroxylated α-Al_2O_3(0001) surfaces. Phys Chem Chem Phys 2014;16:14287–97.

[45] French RH. Electronic Band Structure of Al_2O_3, with Comparison to AlON and AIN. J Am Ceram Soc 1990;73:477–89.

[46] Li J-L, Kudin K, McAllister M, Prud'homme R, Aksay I, Car R. Oxygen-Driven Unzipping of Graphitic Materials. Phys Rev Lett 2006;96:176101.

[47] Fan Z, Wang K, Wei T, Yan J, Song L, Shao B. An environmentally friendly and efficient route for the reduction of graphene oxide by aluminum powder. Carbon 2010;48:1686–9.

[48] Pei S, Zhao J, Du J, Ren W, Cheng HM. Direct reduction of graphene oxide films into highly conductive and flexible graphene films by hydrohalic acids. Carbon 2010;48:4466–74.

[49] Zhu Y, Cai W, Piner RD, Velamakanni A, Ruoff RS. Transparent self-assembled films of reduced graphene oxide platelets. Appl Phys Lett 2009;95:2013–6.